Improved estimation of the global top-of-atmosphere albedo from AVHRR data

Chuan Zhan [a], Shunlin Liang [b,*]

[a] Faculty of Geographical Science, Beijing Normal University, Beijing, 100875, China

[b] Department of Geographical Sciences, University of Maryland, College Park, MD, USA

* Correspondence: sliang@umd.edu; Tel.: +1-301-405-4556

Abstract

The top-of-atmosphere (TOA) albedo, a key component of the earth's energy balance, can be monitored regularly by satellite observations. Compared to the previous study Song et al. (2018), this paper estimates TOA albedo by directly linking Advanced Very High Resolution Radiometer (AVHRR) narrowband reflectance with TOA broadband albedo determined by NASA's Clouds and the Earth's Radiant Energy System (CERES) instead of Moderate Resolution Imaging Spectroradiometer (MODIS). The TOA albedo product developed in this study has an increased spatial resolution, from 1° to 0.05°, and its starting year has been extended from 2000 to 1981, compared to the CERES TOA albedo product. Models of lands and oceans are established separately under different atmospheric and surface conditions using gradient boosting regression tree (GBRT) method instead of the linear regression models in the previous study. The root mean square errors (RMSEs) of the cloudy-sky, clear-sky and snow-cover models over land are 11.2%, 9.2% and 2.3%, respectively; over oceans they are 14.6%, 10.6% and 5.6%, respectively. Compared to Song et al. (2018), the improvements of the three models over land are 28.8%, 29.2% and 68.6%, respectively. Compared to the CERES product, the new product is much more accurate than that from our previous study. The global annual

differences of the TOA albedo obtained with the GBRT product and CERES from 2001 to 2014 are mostly less than 5%.

Key words: TOA albedo; AVHRR; CERES; machine learning; Earth's energy budget.

1. Introduction

The top-of-atmosphere (TOA) albedo plays a significant role in determining Earth's energy balance (Liang et al. 2019; Trenberth et al. 2009; Von Schuckmann et al. 2016). A decrease of only ~0.01 in the global mean albedo is equivalent to the impact of doubling the amount of carbon dioxide in the atmosphere, and a decrease of 0.05 will increase the global surface temperature by ~1 K; thus, it is crucial to accurately estimate the global TOA albedo to obtain a better understanding of the earth's energy budget (North et al. 1981; Wielicki and A. 2005).

To date, many TOA albedo products have been derived from data obtained with broadband sensors (Barkstrom 1984; Duvel et al. 2001; Harries et al. 2005; Loeb et al. 2018; Wielicki et al. 1996). Their applications, however, have been limited by the short temporal coverages of the acquired datasets. Recently, multispectral narrowband sensors have been incorporated to generate relatively high spatial resolution TOA albedo products (Key et al. 2001; Song et al. 2018; Urbain et al. 2017; Wang and Liang 2016, 2017). For example, Key et al. (2001) retrieved TOA albedo by converting narrowband reflectances to broadband reflectance and correcting the TOA broadband reflectance for anisotropy by utilizing data from the Advanced Very High Resolution Radiometer (AVHRR) on board the National Oceanic and Atmospheric Administration (NOAA) polar orbiting satellite. However, their product only covers the Arctic and Antarctic, which limits its application. Similarly, the newly released TOA albedo product from the Climate Monitoring Satellite Application Facility (CM SAF) is also spatially limited (70°N–70°S, 70°W–70°E). This product is generated by combining data from the Meteosat MVIRI and SEVIRI instruments operated by the European Organization for the Exploitation of Meteorological Satellites (EUMETSAT) Data Center, which have 0.05° spatial resolution and cover the years 1983-2015.

Recently, Wang and Liang (2016) retrieved TOA albedo over land from Moderate Resolution Imaging Spectroradiometer (MODIS) data using a hybrid method. To produce a long-term high-resolution time series of TOA albedo, in our previous work (Song et al. 2018) we took the retrieved MODIS TOA albedo as “true values” during the training process, and generated TOA albedo products based on AVHRR data using direct estimation models, which have been widely used to retrieve both surface and TOA albedo (He et al. 2015; Liang et al. 1998; Song et al. 2018; Tang et al. 2006; Wang and Liang 2016). The models are built under clear-sky, snow-cover and cloudy-sky conditions using linear regression, respectively. The previously developed AVHRR TOA albedo (TAL-AVHRR) is the first long-term high spatial resolution TOA albedo product of its kind, but it has two main issues. First, the product is only available over land. Second, its accuracy is relatively low in high-latitude regions. Our recent intercomparison of multiple TOA albedo products showed that the differences between TAL-AVHRR and the other products are relatively large, especially for high latitude regions before the year 2000 (Zhan et al. 2019).

To address these issues, in this current study we have developed a new method to improve TOA albedo estimations from AVHRR data. There are four major improvements over the previous study by Song et al. (2018) (hereinafter S2018). Firstly, machine-learning methods, which have the advantages in fitting nonlinear relationships, are explored to replace the linear fitting. Three common machine-learning methods are adopted for the model building, including multivariate adaptive regression splines (MARS), gradient boosting regression tree (GBRT) and random forest (RF). Secondly, we use the recently released National Oceanic and Atmospheric Administration (NOAA) AVHRR Climate Data Record (CDR). This represents an improvement relative to the AVHRR data (AVH02C1) of the land Long-Term Data Record (LTDR) project, which includes only one observation daily for each pixel. There are many more observations available at high-latitude regions each day in the CDR, which provides the potential to improve the accuracy of its products over the Arctic. Third, the training data are based on the CERES TOA albedo product, which is considered to be the most accurate TOA radiation product available to date, instead of the previously developed MODIS TOA albedo product (TAL-MODIS). Lastly, our methods are applied globally, over both land and ocean surfaces.

The organization of the remainder of this paper is as follows. Section 2 introduces the data used in this study. Detailed algorithm descriptions are presented in Section 3, while Section 4 shows the results and the corresponding analyses. Conclusions are drawn in the final section.

2. Data

2.1 AVHRR

2.1.1 NOAA CDR of Visible and Near Infrared Reflectance

The observed radiances of NOAA CDR of Visible and Near Infrared Reflectance provide the features for the TOA albedo retrieval algorithm. In S2018, the AVHRR TOA reflectance data AVH02C1 obtained from Version 4 of the LTDR project is used. There are three spectral reflectance channels in AVHRR: 0.63 μm (channel 1), 0.86 μm (channel 2), and 1.61 μm (channel 3). In this study, the brightness temperatures of 10.8 μm (channel 4) and 12.0 μm (channel 5) are also used.

2.1.2 NASA Langley Research Center (LaRC) Cloud and Clear Sky Radiation Properties dataset

NASA LaRC Cloud and Clear Sky Radiation Properties dataset (AVHRR Cloud Properties – NASA) is another satellite dataset derived from AVHRR data. It is generated using the CERES Cloud Mask and Cloud Property Retrieval System. The algorithm is initially designed for application to the Tropical Rainfall Measurement Mission (TRMM) and MODIS data within the CERES program. It provides many atmospheric and land surface variables, such as cloud masks, snow and ice cover flags, cloud optical depth, cloud top air temperature, cloud base air temperature, cloud top height, cloud base height, shortwave broadband albedo and longwave broadband flux. Cloud masks and snow and ice cover flags are used to identify the cloudy and snow-covered pixels.

2.2 CERES

CERES is a broadband instrument onboard TRMM, Terra, Aqua, Suomi National Polar-orbiting Partnership (Suomi NPP) and NOAA-20, which measures shortwave reflected radiation (0.3–5 μm), longwave thermal radiation (8–12 μm) and broadband radiation from 0.3–

200 μm (Wielicki et al. 1998). The CERES shortwave fluxes have been developed using angular distribution models (Loeb et al. 2005; Loeb et al. 2003; Su et al. 2015), while the Level-2 Single Scanner Footprint (SSF) provides instantaneous TOA albedo at a resolution of 20 km (Doelling et al. 2013). This study takes CERES SSF data as labels for the machine learning models, while in S2018 MODIS TOA albedo are taken as "true values". Currently, the CERES fluxes are considered to be the most accurate coarse-resolution products. Additionally, the Level-3 Synoptic products (i.e., the SYN1deg data) (Doelling et al. 2013), which consist of hourly and daily/monthly mean TOA radiative fluxes, are used as reference values in both S2018 and this study. They began in March 2000 with a resolution of 1 degree, and we used their latest version Edition4A, released during September 2017.

2.3 MERRA-2

Modern-Era Retrospective analysis for Research and Applications, Version 2 (MERRA-2) is developed as an Earth System reanalysis product (Gelaro et al. 2017). It provides global dynamic and meteorological fields from 1980 to the present with a spatial resolution of 0.5 × 0.625 degrees. It consists of 42 collections that contain multiple variables, and has been used for a variety of climate research and renewable energy studies (Wargan and Coy 2016). In S2018, they used the linear regression models, so MERRA-2 dataset is not used. In this study, two MERRA-2 variables are used as the input feature of the machine learning models: (1) TOA incoming shortwave flux (SWTDN), and (2) TOA net downward shortwave flux (SWTNT). MERRA-2 observing system includes atmospheric motion vectors from AVHRR, and AOD observations are also derived from AVHRR reflectances. Despite its uncertainty, the inclusion of MERRA-2 dataset can reduce the training uncertainties by providing initial values of the TOA albedo in the training process.

3. Algorithm Description

Fig. 1 shows a flowchart of the method used to estimate the TOA broadband albedo from AVHRR CDR. It consisted of three major steps. First, both the AVHRR CDR and CERES SSF data are pre-processed. The pre-process includes converting both the AVHRR swath data and CERES SSF data to the 20-km regular gird. Then, the TOA reflectances and brightness temperatures are extracted from the AVHRR data, and the corresponding TOA albedo are obtained from the MERRA-2 and CERES SSF data. Meanwhile, the corresponding solar/viewing geometries and observation times of the AVHRR and CERES datasets are also extracted. Second, a training dataset containing 2,513,556 samples is established from coincident AVHRR observations and the CERES TOA albedo product. The criteria of collecting AVHRR-CERES data pairs includes: (1) the difference in the acquisition time between the two data sets is limited to 5 minutes, (2) the differences of the solar zenith angle and viewing zenith angle are less than 5 degrees and the differences of the relative azimuth angle are less than 30 degrees, (3) two datasets are collocated with the same spatial scale of 20 km. Essentially, only data pairs that are consistent in timing, spatial scale, and solar-viewing geometry are used in the analysis. To ensure the training data pairs are representative, we collected 12 months of global collocated AVHRR and CERES data from 2007. In total, 895,257 data pairs are collected for land, which covered various surface types and atmospheric conditions, and 1,618,299 data pairs are collected for the ocean model construction. The dataset is randomly stratified into two groups, where 90% is used for training dataset and the remaining 10% formed the testing dataset. Finally, models are built based on the training dataset with cloud/snow/land masks using machine-learning methods. We evaluated different approaches (MARS, GBRT, RF) and found GBRT to provide the best results. Thus, we obtained cloudy-sky, clear-sky (non-snow), and clear-sky (snow) models, where each model is also separated into land and ocean models based on the land mask. The sample number of different models is shown in Table 1. For the clear-sky and cloudy-sky models, the former is defined as no cloud coverage, while conditions with cloud fractions larger than 0% are used for the latter. Furthermore, considering the unique bidirectional reflectance distribution function (BRDF) characteristics of snow-covered surfaces, snow masks from the AVHRR data are used to build the clear-sky snow-covered models separately.

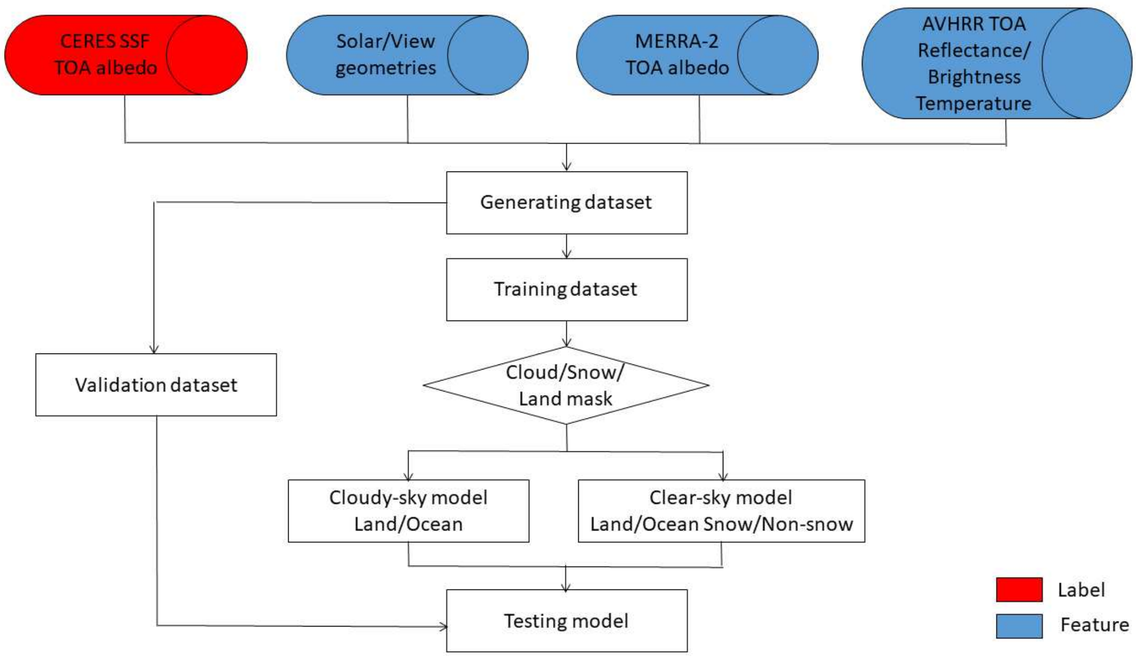

Fig. 1. Flowchart of TOA broadband albedo estimation from AVHRR CDR.

Table 1. Sample number of different models

	Cloudy-sky	**Clear-sky (Snow)**	**Clear-sky (Non-snow)**

Land	545023	286506	63728
Ocean	1488076	54766	75457

Reanalysis products, which are usually derived by merging available observations with atmospheric models to obtain best estimates of the states of the atmosphere and land, also served as model features in this study. Although reanalysis products are not as accurate as satellite products, they allowed us to refine GBRT results using different data sources. The corresponding MERRA-2 TOA albedo values are obtained by interpolation based on the observation time, and they are used to provide an initial value or first guess for the model. MERRA-2 is chosen among the common reanalysis products as it has a relatively high temporal resolution (1 hour). The TOA albedo is used as model features, which is calculated as:

$$Albedo = (\mathrm{SWTDN} - \mathrm{SWTNT})/\mathrm{SWTDN} \quad (1)$$

As daily TOA albedo play a more important role in analyzing Earth’s energy budget than instantaneous TOA albedo, conversion ratios are needed to convert the latter to the former. They are needed due to diurnal variations in TOA albedo caused by underlying atmospheric or surface properties (Gristey et al. 2018; Rutan et al. 2014). S2018 proposed two kinds of conversion ratios: (1) real-time conversion ratios and (2) climatology conversion ratios, both of which are based on CERES three-hourly flux data and daily flux data. However, as the CERES data are not available before 2000, the real-time conversion ratios did not meet the needs of this study. Therefore, the climatology conversion ratios are used in this study. The climatology conversion ratios are derived from multi-year CERES flux data from 2001 to 2017 using Equation (2), in which $\mathrm{F}_{sw-up}^{daily}$ is the daily mean shortwave upward flux and $\mathrm{F}_{sw-up}^{instan}$ is the instantaneous shortwave upward flux. r and b, which depend on the location and day of year, are the climatology conversion ratios derived by linear regressions. Compared to S2018, the ratios are updated using CERES hourly data instead of the three-hourly data. After the instantaneous TOA albedo is obtained, instantaneous shortwave upward flux can be derived by multiplying with instantaneous shortwave downward flux. Then, daily mean shortwave upward flux can be calculated from Equation (2). Finally, daily TOA albedo can be obtained by dividing it by the daily mean shortwave downward flux.

$$\mathrm{F}_{sw-up}^{daily} = r * \mathrm{F}_{sw-up}^{instan}(t) + b \quad (2)$$

4. Results and analysis

4.1 Instantaneous results

The test results over land and oceans using GBRT are shown in Fig. 2. It compares the results obtained with the estimated instantaneous TOA albedo and the CERES SSF TOA albedo, the latter of which are taken as labels in the training process. The RMSEs of the GBRT land model under clear-sky, snow-cover and cloudy-sky conditions are 9.217%, 2.281% and 11.153%, respectively, while over ocean they are 10.586%, 5.644%, and 14.648%. From these six sub-figures, one can see that there are high-density TOA albedo values around 0.2 for clear-sky and cloudy-sky conditions. For cloudy-sky conditions, this relatively low value can be attributed to false positive cloud detections or correct cloud detection for rather thin clouds, where the surface albedo shines through. For the snow-cover model, the values under this condition are even lower than under the clear-sky condition. This makes sense as there are various surface types under clear-sky conditions.

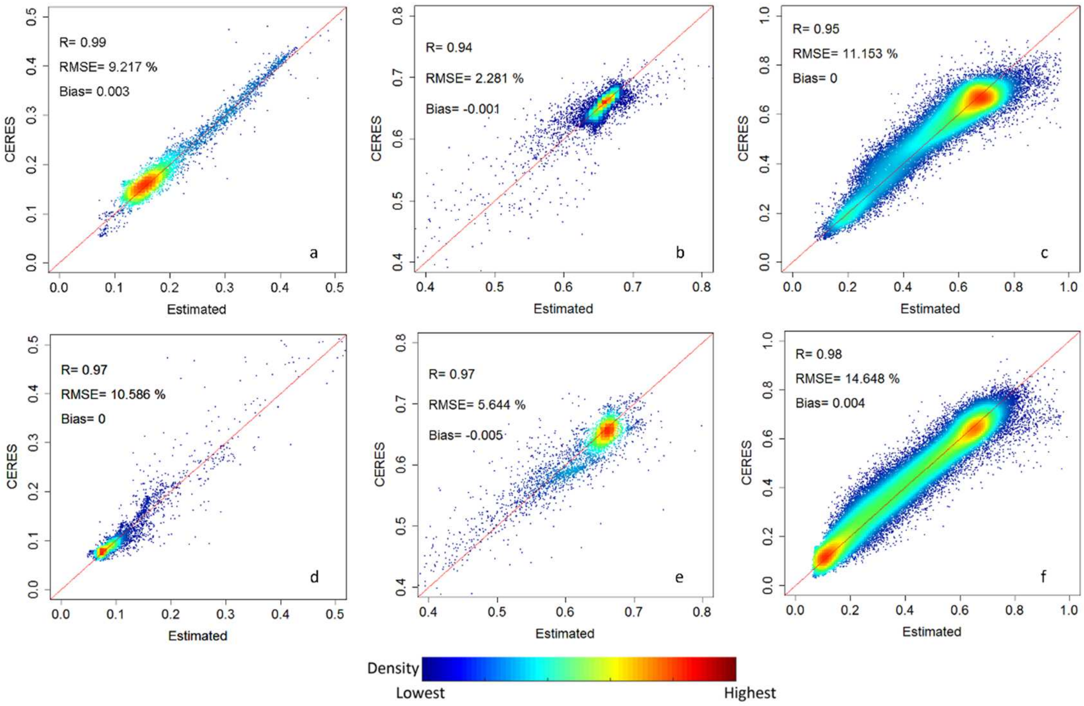

Fig. 2. Test results of the TOA albedo derived from the GBRT models for (a) clear land (b) snow-cover land (c) cloudy land (d) clear ocean (e) ice-cover ocean (f) cloudy ocean.

4.2 Daily time series results

After obtaining the instantaneous TOA albedo, we converted them into daily values using the conversion ratios. Note that AVHRR CDR provides multiple observations for high latitude regions (~14 per day), which we averaged to obtain the final daily values.

To show the improvements found here compared to S2018, time series of both results in 2008 are presented in Fig. 3. From Fig. 3, one can see that greater improvements have been made in high latitude regions. In Fig. 3(a), the differences between the results of S2018 and CERES can be as large as 0.05 in winter, while the differences between GBRT results and CERES are mostly less than 0.02. Similar results can be found in Fig. 3(b), which illustrates the obvious underestimation of the results of S2018 in the Northern Hemisphere in winter. Over

Antarctic, as shown in Fig. 3(f), overestimations are found in the results of S2018 during the first 30 days of year, while during the last 40 days of year there are obvious underestimations. GBRT results, nevertheless, showed good consistency with the CERES data. The reason for the jump around 50 days of the year in S2018 is that the MODIS TOA albedo, which are taken as "true values" in the previous training process, contain large uncertainties in the Antarctica. As we have replaced it with CERES TOA albedo, the discontinuity is resolved. Additionally, 14 daily observations of the AVHRR data in the Antarctica also contribute to the improvement. Note that there is no sunlight in this region in the summer. Therefore, we only considered the first 90 days of year for the comparison.

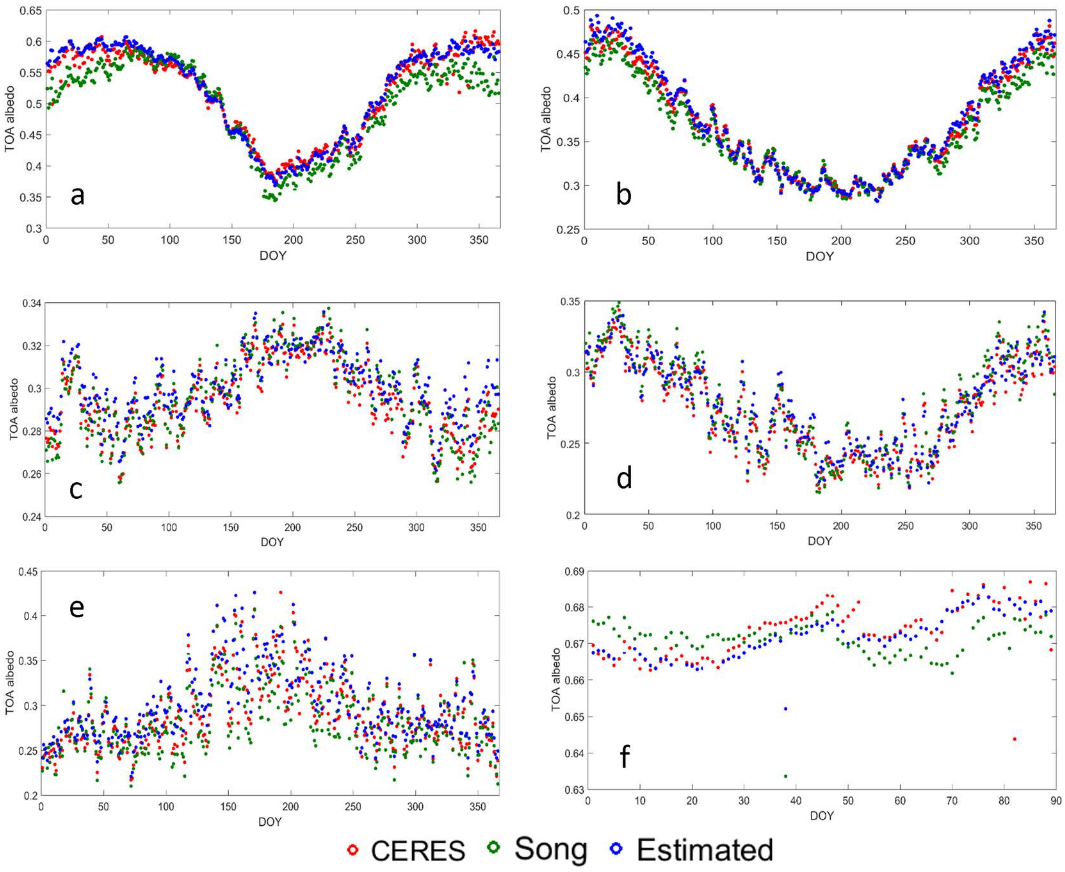

Fig. 3. Time series of the daily TOA albedo values from CERES (red), S2018 (green), and this study (blue) in 2008 for the following latitude regions: (a) 60–90° N, (b) 30–60° N, (c) 0–30° N, (d) 0–30°

S, (e) 30–60° S, and (f) 60–90° S.

Additionally, comparisons for years after 2000, when CERES data are available, are presented in Fig. 4. The mean difference (MD) and standard deviation (STD) between the estimated daily results and CERES data since January 1, 2001 are shown in the figure. Overall, there are positive biases in GBRT results when the CERES data are taken as reference, while negative biases with greater magnitudes are found in the results of S2018, especially from 2001 to 2005. Similarly, improvements are visible in the STD time series, where GBRT results are significantly lower compared to the S2018 data. The TOA albedo products of Song et al. (2018) contain large uncertainties in the high-latitude regions, especially during June to August. Thus, STD increases in these months, and a large annual cycle is shown. For the GBRT results, No annual cycle is obvious in the mean difference, but there is a visible annual cycle in STD, which is smaller than the S2018 results.

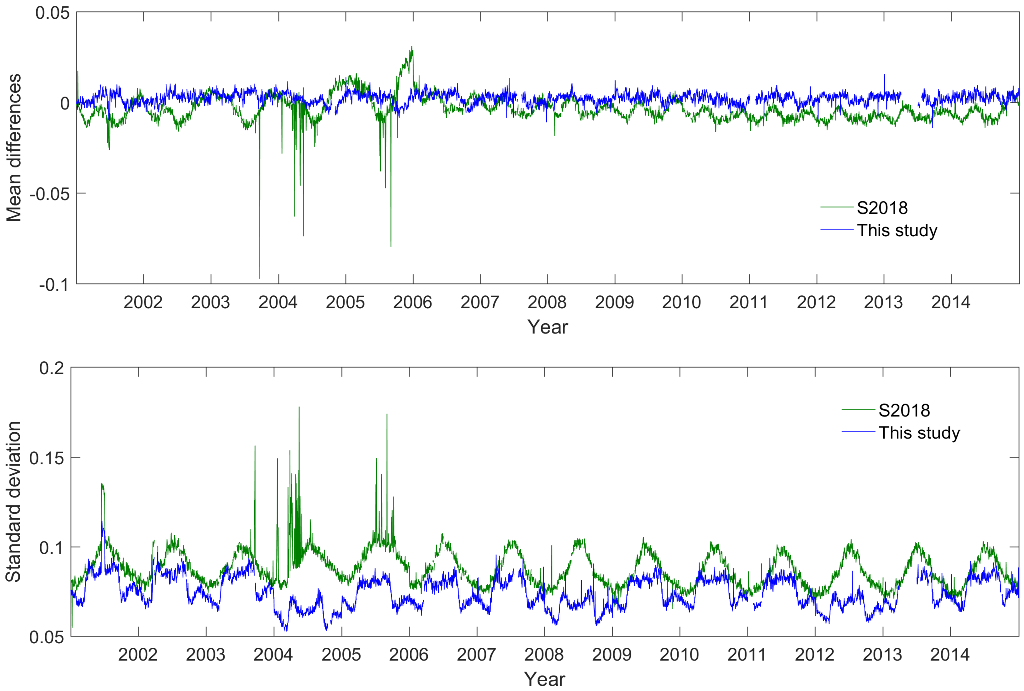

Fig. 4. Mean difference (MD) and standard deviation (STD) between the estimated daily results from this study, as well as S2018, and the CERES product over land since 2001.

4.3 Monthly results

Compared to the daily TOA albedo, monthly products are more widely used when analyzing the long-term changes of the earth's energy budget. Therefore, monthly results are obtained by averaging the daily results. Estimated monthly TOA albedo values and the differences from CERES SYN TOA albedo in January and July, 2008 are shown in Fig. 5. The results of S2018 are also plotted to illustrate the improvements found here.

In Figs. 5(a) and 5(b), the north and south pole stand out due to their snow or ice cover, and the values of low-latitude ocean are relatively low. By comparing Figs. 5(c) and 5(e), we can see large improvements found in the Antarctic, while in other regions the improvements are only slight. It is worth noting that the Arctic has no data in January while the Antarctic has no data in July because of the lack of sunlight. In July, as shown in Figs. 5(b) and 5(d), there are obvious improvements in high-latitude regions in the Northern Hemisphere. The underestimations in the results of S2018 are reduced in GBRT results. Additionally, it is worth noting that the uncertainties over the ocean can be as high as 100%. For example, in Figure 5c, the low albedo area in the Indian Ocean (~0.1-0.2) exhibits differences to the CERES data in the range of ~0.1. These uncertainties may attribute to sun glint, and uncertainties in the cloud flagging have a much larger effect on these low-albedo areas.

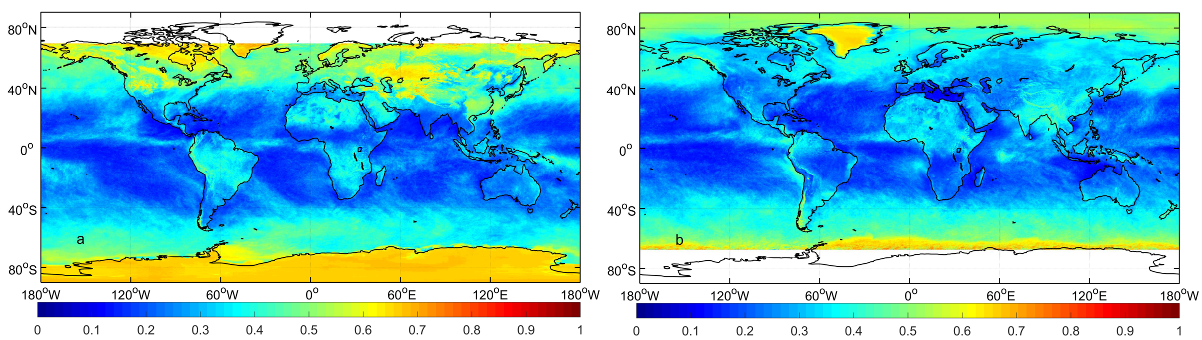

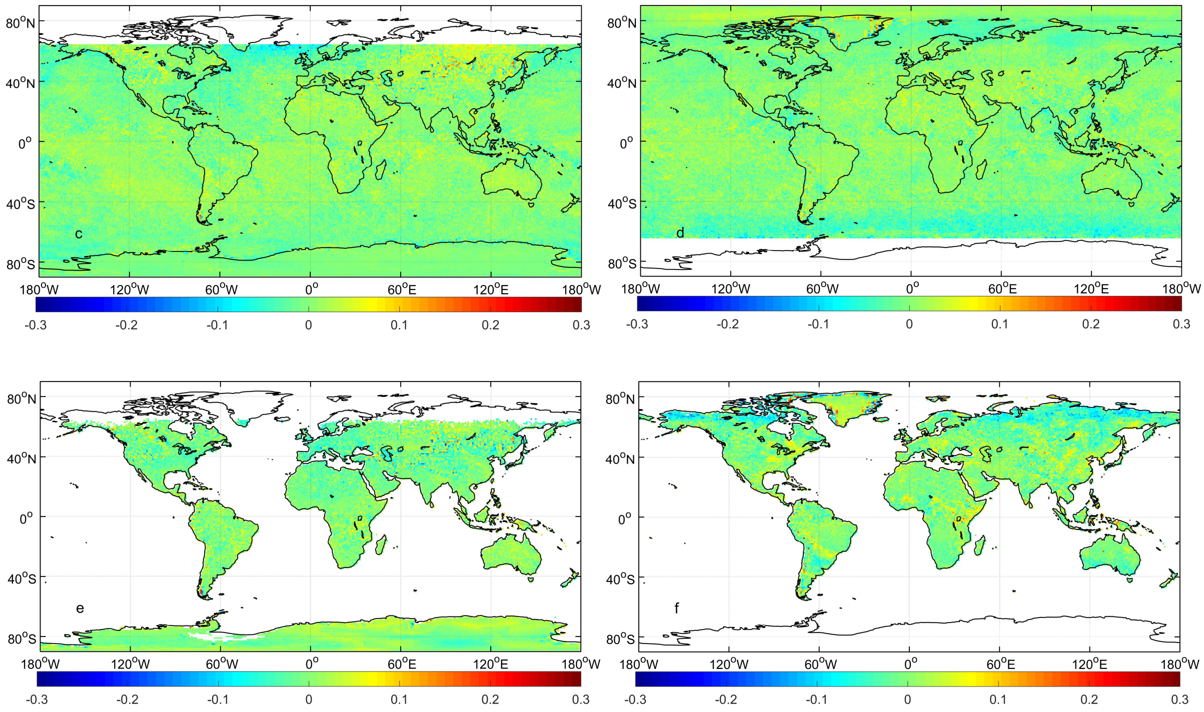

Fig. 5. Estimated monthly TOA albedo values and the differences from the CERES SYN TOA albedo in January, 2008 (a) estimated monthly TOA albedo (c) differences of this study (e) differences of S2018, (b), (d) and (f) are the same but for July, 2008.

The RMSEs of GBRT results over land are 7.05% and 8.03% for the two months used in this study, respectively, which are lower than those of S2018, where the RMSEs are 7.76% and 12.80%, respectively. Over ocean, the RMSEs are 7.55% and 7.72% for January and July, and the biases are -1.14% and -0.36%, respectively. In panel a, the S2018 results exhibit a slight negative bias (-0.47%), while the new product exhibits a slight positive bias (1.68%). In panel b, S2018 has a slight negative bias (-1.80%), while the new product has a slight positive bias (1.44%). The TOA albedo estimates over oceans are one of the benefits of the new algorithm. Judging from the results of the two months, it can be concluded that the monthly TOA albedo can meet the need of long-term Earth's energy budget analysis.

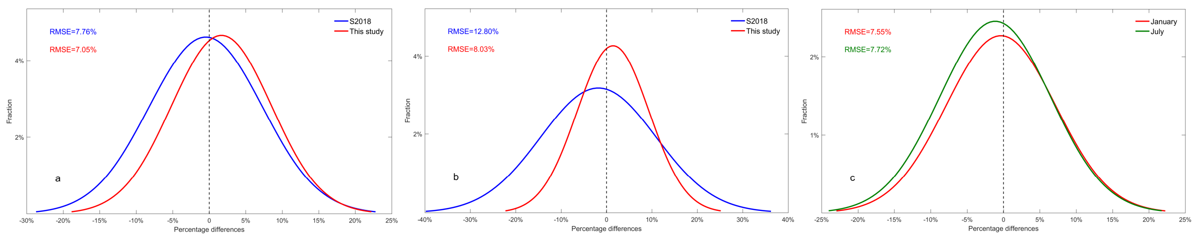

Fig. 6. Fraction of the percentage differences shown in Fig. 5. (a) January, 2008 of land, (b) July, 2008 of land and (c) January and July, 2008 of ocean.

As the advantage of the AVHRR dataset is its long time span, it is beneficial to make comparisons between the TOA albedo from the different datasets for years before 2000. Here, the Diagnosing Earth's Energy Pathways in the Climate system (DEEP-C) product, which covers the period before 2000, has been included in the intercomparison (Allan et al. 2014). Fig. 7 shows a time series of the DEEP-C, S2018, and our monthly mean TOA albedo, as well as the percentage differences in the maritime continent region in which significant differences are found among different TOA albedo products in Zhan et al. (2019). Compared with the S2018 results, ours are much closer to the DEEP-C values.

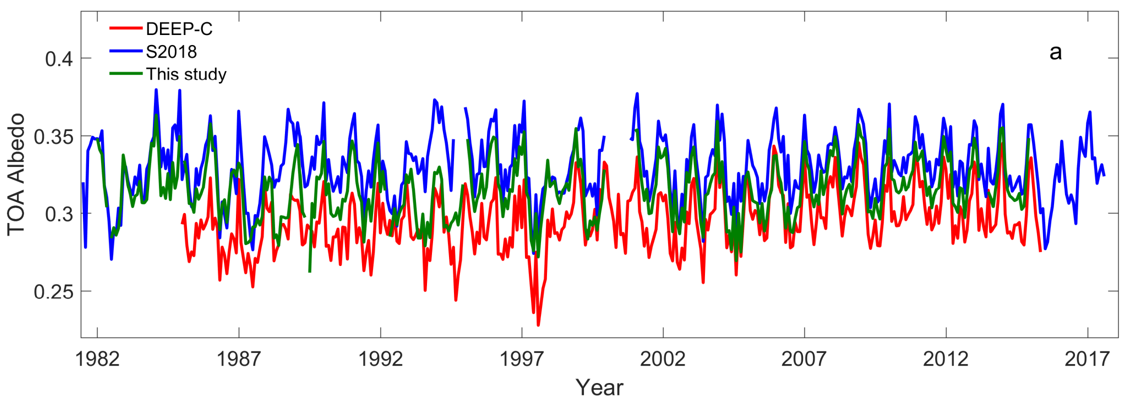

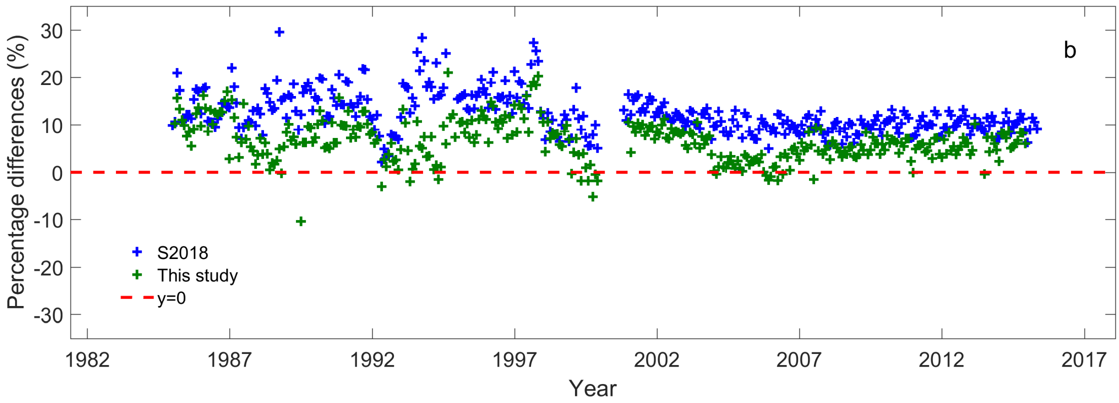

Fig. 7. Time series of (a) three monthly mean TOA albedo values and (b) the percentage differences from DEEP-C in MCT region.

Additionally, Fig. 8 shows the global monthly differences between the TOA albedo found with new product and the CERES results. Good consistency can be seen in terms of the TOA albedo anomalies, and the percentage differences are mostly within 5%. Compared to the CERES TOA albedo product, we not only increased the spatial resolution from 1° to 0.05°, but also extended the starting year from 2000 to 1981.

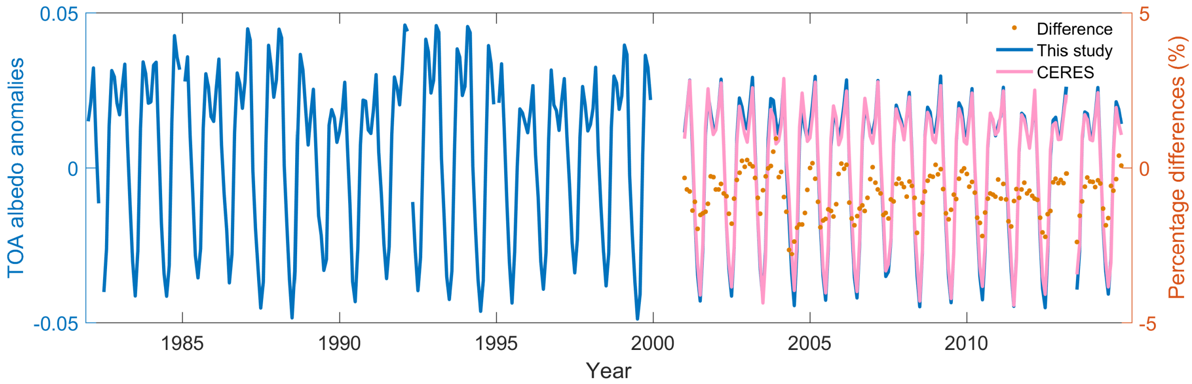

Fig. 8. AVHRR and CERES global monthly mean TOA albedo anomalies. The percentage differences are calculated between the AVHRR and CERES monthly mean TOA albedo in the overlapping period from 2001 to 2014.

5. Discussion

5.1 Incorporation of thermal bands and MERRA-2 data in the training process

One of the improvements here compared to S2018 is the incorporation of thermal bands and MERRA-2 data when building the training dataset. Additional experiments are conducted in this section to show the impact of the additional datasets. Here, the thermal bands and MERRA-2 data are separately removed from the training dataset. Then, we calculated the corresponding RMSEs with and without these datasets. The results are shown in Tables 2. From the table, one can see that the RMSEs generally increase when either the thermal bands or MERRA-2 TOA albedo are removed. For cloudy-sky model, however, the incorporation of MERRA-2 TOA albedo does not take effect, which may attribute to the variation of clouds in a short period. For the other two models over land, greater improvements could be achieved when the MERRA-2 data are incorporated compared to the incorporation of the thermal bands.

Table 2. RMSE and bias values of the test results for the three models under the different conditions

		With both		**Without MERRA-2**		**Without thermal bands**	
		RMSE	**Bias**	**RMSE**	**Bias**	**RMSE**	**Bias**
Cloudy-sky model	Ocean	14.65%	0.004	14.65%	0.004	14.78%	0.005
	Land	11.15%	0	11.15%	0	11.37%	0.001
Clear-sky model	Ocean	10.59%	0	10.68%	0	11.49%	-0.002
	Land	9.21%	0.003	9.49%	0.004	9.22%	0.003
Snow/ice-cover model	Ocean	5.64%	-0.005	6.54%	-0.006	5.64%	-0.005
	Land	2.28%	-0.001	2.44%	-0.003	2.30%	-0.002

S2018 only used two bands of the AVHRR data, namely the visible band (0.580–0.680 μm) and near-infrared band (0.725–1.100 μm). By incorporating the thermal bands, we not only provided more information for the model building, but changed the mechanism of the algorithm, which made full use of the connections among the different bands, through the visible bands to the thermal bands, and the results exhibited some slight improvements. The incorporation of

MERRA-2 data is, however, more useful. As a widely used reanalysis dataset, MERRA-2 covers long time period and has relatively high spatial resolution. It can provide, as done here, first guess values in cases where the quality of the AVHRR data are relatively poor, especially before the year 2000. Additionally, it is worth noting that this study makes predictions of TOA albedo using CERES SSF instead of MODIS TOA albedo as the "truth values", and then evaluated against CERES SYN. Thus, the evaluation of the S2018 approach is largely independent, whereas the evaluation for the new method is not independent, which may have impacted the findings in this study.

5.2 Selection of instantaneous-to-daily conversion ratios

The uncertainties of the daily TOA albedo retrieved in this study mainly arise from the instantaneous-to-daily conversion process. Large uncertainties (~0.2) are reported by S2018 in terms of daily results. The climatology conversion ratios obtained from linear regression models are unable to capture some real-time changes. Instead, the real-time conversion ratios applied to the CERES data are able to provide more accurate diurnal variations as they depend on real-time observations, but they are not available before the year 2000. Considering the long time span of the currently available reanalysis datasets, here we also developed real-time conversion ratios based on two popular reanalysis datasets (i.e., MERRA-2 and ERA5).

The temporal resolutions of MERRA-2 and ERA-5 (1-hour) are higher than the other reanalysis datasets, which greatly contributed to the usability of the developed conversion ratios. Following the scheme of S2018, real-time conversion ratios based on the two datasets are obtained by building a look-up table for every hour in a day and for observation time *t*. Table 3 shows the RMSE and bias values of four daily average results (first day of January, April, July and October in 2008) using different conversion ratios. In addition to the higher RMSEs, notable negative biases are also found in the results obtained via the reanalysis data-based conversion ratios. The biases are -3.79% and -3.55% for ERA-5 and MERRA-2, respectively, which are higher than those found via the climatology conversion ratios, as the reanalysis dataset may not capture the diurnal cycle correctly. Therefore, we still choose the climatology conversion ratios when generating the TOA albedo products. Actually, the climatology ratios became more usable after using the CERES hourly data instead of the three-hourly data.

Table 3. RMSE and bias values of four daily average results using different conversion ratios

	CERES climatology ratio	**ERA-5 real-time ratio**	**MERRA-2 real-time ratio**
RMSE	26.51%	29.75%	28.17%
Bias	1.20%	-3.79%	-3.55%

5.3 Effects of sun glint over ocean surface

Sun glint, a phenomenon that occurs when sunlight reflects off the ocean surfaces at the same angle that a satellite sensor views the surface, may induce extra biases in the retrieval process in this study. To analyze the effects of sun glint over ocean surface, the glint angle, which indicates the intensity of sun glint, is used here. The glint angle is defined as:

$$\theta_{glint} = \cos^{-1}(\cos\theta_s \cos\theta_v + \sin\theta_s \sin\theta_v \cos\varphi) \quad (3)$$

where θ_{glint} is the glint angle, and θ_s ,θ_v and φ are solar zenith angle, viewing zenith angle, and relative azimuth angle, respectively.

As the intensity of sun glint is larger when the glint angle is smaller (largest when glint angle equals 0), we remove the samples with small glint angles to illustrate the effects of sun glint. The thresholds are set to 0, 10, 20, 30 and 40 degrees, and the corresponding RMSE and bias are shown in Table 4. From this table, one can see that the RMSEs become even larger when the samples with smallest glint angles (less than 10°) are removed, which illustrates that the impact of sun glint on algorithm performance is small. Note that by filtering out more data we reduce the sample size, which may negatively impact the model performance.

Table 4. Statistics of the results when the samples with small glint angles are removed, using different thresholds

Threshold	Number	RMSE	Bias
/	75457	10.59%	0
10	50860	10.74%	0
20	29276	11.13%	0.001
30	13782	10.85%	0.001
40	6039	10.88%	0.003

6. Conclusion

The global TOA albedo is a key component of the earth's energy budget, and most TOA albedo products have been developed from data acquired by broadband satellite sensors. In this study, a robust machine-learning-based method for estimating TOA albedo based on AVHRR data is proposed, which provides a unique global data source since 1981. Instead of typical two-step methods, we use a direct estimation method, the essence of which is to estimate albedo from spectral information by establishing a relationship between TOA multispectral reflectances and TOA albedo. The GBRT machine-learning method is used for model building. The CERES SSF TOA albedo product provides the labels, and land masks are used to build land and ocean models separately. Instantaneous TOA albedo are derived from each of these models, and daily TOA albedos are obtained by multiplying the instantaneous results by climatology conversion ratios that are based on the CERES daily and hourly TOA albedo.

The test results show that the RMSEs of the cloudy-sky, clear-sky and snow-cover models over land are 11.2%, 9.2% and 2.3%, respectively; they are 14.6%, 10.6% and 5.6% over oceans. Additionally, incorporation of thermal bands and the MERRA-2 TOA albedo is quite necessary in the training process, as the estimation accuracy generally decreased if they are removed. For the monthly results, intercomparisons are made among three products, including the widely-used CERES data, GBRT results and the AVHRR TOA albedo estimated by S2018. The comparisons show that the differences between GBRT results and the CERES data are significantly reduced in high-latitude regions when compared with the results of S2018. Over oceans, the accuracy of GBRT results are similar to those found over land. Time series show that great improvements are made, especially for high-latitude and maritime continent regions compared to S2018.

Despite the good progress made here, our method still has some room for improvement. The climatology conversion ratios are not perfect ratios for converting instantaneous results to daily results, as demonstrated by the large errors found in low-latitude regions (e.g., the tropics) where multiple daily observations from AVHRR are unavailable. Future work may incorporate geostationary estimates to more accurately characterize diurnal variations of the TOA albedo values, which will improve the accuracy of the daily TOA albedo estimations.

Acknowledgements

This study is partially funded by the National Key Research and Development Program of China (NO.2016YFA0600101). We thank for the data support from "National Earth System Science Data Center, National Science & Technology Infrastructure of China" (http://www.geodata.cn). The CERES datasets are downloaded at https://ceres-tool.larc.nasa.gov/ord-tool/jsp/SYN1degEd4Selection.jsp. The previous version of the TAL-AVHRR is produced and updated in August 2017 and the datasets are distributed at http://www.geodata.cn/ and http://glcf.umd.edu/data. The TOA albedo product from this study will also be distributed at these two web sites. The AVHRR CDR data are downloaded at https://www.ncdc.noaa.gov/cdr, and the MERRA-2 data can be downloaded at https://gmao.gsfc.nasa.gov/reanalysis/merra-2. We would like to thank the anonymous reviewers for their constructive comments and suggestions.

References

Allan, R.P., Liu, C., Loeb, N.G., Palmer, M.D., Roberts, M., Smith, D., & Vidale, P.L. (2014). Changes in global net radiative imbalance 1985–2012. *Geophysical research letters, 41*, 5588-5597

Barkstrom, B.R. (1984). The earth radiation budget experiment (ERBE). *Bulletin of the American Meteorological Society, 65*, 1170-1185

Cox, C., & Munk, W. (1954). Measurement Of The Roughness Of The Sea Surface From Photographs Of The Suns Glitter. *Journal of the Optical Society of America, 44*, 838-850

Doelling, D.R., Loeb, N.G., Keyes, D.F., Nordeen, M.L., Morstad, D., Nguyen, C., Wielicki, B.A., Young, D.F., & Sun, M. (2013). Geostationary enhanced temporal interpolation for CERES flux products. *Journal of Atmospheric and Oceanic Technology, 30*, 1072-1090

Duvel, J.-P., Viollier, M., Raberanto, P., Kandel, R., Haeffelin, M., Pakhomov, L., Golovko, V., Mueller, J., Stuhlmann, R., & Group, I.S.S.W. (2001). The ScaRaB-Resurs Earth radiation budget dataset and first results. *Bulletin of the American Meteorological Society, 82*, 1397-1408

Gelaro, R., Mccarty, W., Suárez, M.J., Todling, R., & Zhao, B. (2017). The Modern-Era Retrospective Analysis for Research and Applications, Version 2 (MERRA-2). *Journal of Climate, 30*

Gristey, Jake, J., Chiu, Christine, J., Gurney, Robert, J., Morcrette, Cyril, J., Hill, & Peter, G. (2018). Insights into the diurnal cycle of global Earth outgoing radiation using a numerical weather prediction model. *Atmospheric chemistry and physics*

Harries, J.E., Russell, J., Hanafin, J., Brindley, H., Futyan, J., Rufus, J., Kellock, S., Matthews, G., Wrigley, R., & Last, A. (2005). The geostationary earth radiation budget project. *Bulletin of the American Meteorological Society, 86*, 945-960

He, T., Liang, S., Wang, D., Chen, X., Song, D.-X., & Jiang, B. (2015). Land surface albedo estimation from Chinese HJ satellite data based on the direct estimation approach. *Remote Sensing, 7*, 5495-5510

Key, J.R., Wang, X., Stoeve, J.C., & Fowler, C. (2001). Estimating the cloudy‐sky albedo of sea ice and snow from space. *Journal of Geophysical Research: Atmospheres, 106*, 12489-12497

Liang, S., Strahler, A.H., & Walthall, C. (1998). Retrieval of land surface albedo from satellite observations: a simulation study. In, *IEEE International Geoscience & Remote Sensing Symposium*

Liang, S., Wang, D., He, T., & Yu, Y. (2019). Remote sensing of earth's energy budget: synthesis and review. *International Journal of Digital Earth, 12*, 737-780

Loeb, N.G., Doelling, D.R., Wang, H., Su, W., Nguyen, C., Corbett, J.G., Liang, L., Mitrescu, C., Rose, F.G., & Kato, S. (2018). Clouds and the earth's radiant energy system (CERES) energy balanced and filled (EBAF) top-of-atmosphere (TOA) edition-4.0 data product. *Journal of Climate, 31*, 895-918

Loeb, N.G., Kato, S., Loukachine, K., & Manalo-Smith, N. (2005). Angular Distribution Models for Top-of-Atmosphere Radiative Flux Estimation from the Clouds and the Earth's Radiant Energy System Instrument on the Terra Satellite. Part Ⅰ: Methodology. *Journal of Atmospheric and Oceanic Technology, 22*, p.338-351

Loeb, N.G., Manalo-Smith, N., Kato, S., Miller, W.F., Gupta, S.K., Minnis, P., & Wielicki, B.A. (2003). Angular distribution models for top-of-atmosphere radiative flux estimation from the Clouds and the Earth's Radiant Energy System instrument on the Tropical Rainfall Measuring Mission satellite. Part I: Methodology. *Journal of applied meteorology, 42*, 240-265

North, G.R., Cahalan, R.F., & Coakley, J.A. (1981). Energy balance climate models. *Reviews of Geophysics, 19*

Rutan, David, A., Smith, Louis, G., Wong, & Takmeng (2014). Diurnal Variations of Albedo Retrieved from Earth Radiation Budget Experiment Measurements. *Journal of Applied Meteorology & Climatology, 53*, 2747-2760

Song, Z., Liang, S., Wang, D., Zhou, Y., & Jia, A. (2018). Long-term record of top-of-atmosphere albedo over land generated from AVHRR data. *Remote Sensing of Environment, 211*, 71-88

Su, W., Corbett, J., Eitzen, Z., Liang, & L. (2015). Next-generation angular distribution models for top-of-atmosphere radiative flux calculation from the CERES instruments: validation. *Atmospheric Measurement Techniques Discussions*

Tang, B., Li, Z.-L., & Zhang, R. (2006). A direct method for estimating net surface shortwave radiation from MODIS data. *Remote Sensing of Environment, 103*, 115-126

Trenberth, K.E., Fasullo, J.T., & Kiehl, J. (2009). Earth's global energy budget. *Bulletin of the American Meteorological Society, 90*, 311-324

Urbain, M., Clerbaux, N., Ipe, A., Tornow, F., Hollmann, R., Baudrez, E., Velazquez Blazquez, A., & Moreels, J. (2017). The CM SAF TOA radiation data record using MVIRI and SEVIRI. *Remote Sensing, 9*, 466

Von Schuckmann, K., Palmer, M., Trenberth, K., Cazenave, A., Chambers, D., Champollion, N., Hansen, J., Josey, S., Loeb, N., & Mathieu, P.-P. (2016). An imperative to monitor Earth's energy imbalance. *Nature Climate Change, 6*, 138

Wang, D., & Liang, S. (2016). Estimating high-resolution top of atmosphere albedo from Moderate Resolution Imaging Spectroradiometer data. *Remote Sensing of Environment, 178*, 93-103

Wang, D., & Liang, S. (2017). Estimating Top-of-Atmosphere Daily Reflected Shortwave Radiation Flux Over Land From MODIS Data. *IEEE Transactions on Geoscience & Remote Sensing, PP*, 1-10

Wargan, K., & Coy, L. (2016). Strengthening of the Tropopause Inversion Layer During the 2009 Sudden Stratospheric Warming: A MERRA-2 Study. *Journal of the Atmospheric ences*, 160205104146006

Wielicki, & A., B. (2005). Changes in Earth's Albedo Measured by Satellite. *Science, 308*, 825

Wielicki, B.A., Barkstrom, B.R., Baum, B.A., Charlock, T.P., Green, R.N., Kratz, D.P., Lee, R.B., Minnis, P., Smith, G.L., & Wong, T. (1998). Clouds and the Earth's Radiant Energy System (CERES): algorithm overview. *IEEE Transactions on Geoscience and Remote Sensing, 36*, 1127-1141

Wielicki, B.A., Barkstrom, B.R., Harrison, E.F., Lee III, R.B., Smith, G.L., & Cooper, J.E. (1996). Clouds and the Earth's Radiant Energy System (CERES): An earth observing system experiment. *Bulletin of the American Meteorological Society, 77*, 853-868

Zhan, C., Allan, R.P., Liang, S., Wang, D., & Song, Z. (2019). Evaluation of five satellite top-of-atmosphere albedo products over land. *Remote Sensing, 11*, 2919